3-10-2017

Magnetochromic sensing and size-dependent collective excitations in iron oxide nanoparticles

Kenneth Robert O'Neal
koneal5@vols.utk.edu

J M. Patete
State University of New York at Stony Brook

P Chen
University of Tennessee, Knoxville

R Nanavati
State University of New York at Stony Brook

Brian S. Holinsworth
University of Tennessee, Knoxville

See next page for additional authors

Magnetochromic sensing and size-dependent collective excitations in iron oxide nanoparticles

Kenneth R. O'Neal,[1] Jonathan M. Patete,[2] Peng Chen,[1] Ruhani Nanavati,[2] Brian S. Holinsworth,[1] Jacqueline M. Smith,[2] Carlos Marques,[3] Jack W. Simonson,[4] Meigan C. Aronson,[3,5] Stephen A. McGill,[6] Stanislaus S. Wong,[2,5] and Janice L. Musfeldt[1,7,*]

[1]*Department of Chemistry, University of Tennessee, Knoxville, Tennessee 37996, USA*
[2]*Department of Chemistry, State University of New York at Stony Brook, Stony Brook, New York 11794-3400, USA*
[3]*Department of Physics and Astronomy, Stony Brook University, Stony Brook, New York 11794-3800, USA*
[4]*Department of Physics, Farmingdale State College, Farmingdale, New York 11735, USA*
[5]*Condensed Matter Physics and Materials Science Division, Brookhaven National Laboratory, Upton, New York 11973, USA*
[6]*National High Magnetic Field Laboratory, Tallahassee, Florida 32310, USA*
[7]*Department of Physics, University of Tennessee, Knoxville, Tennessee 37996, USA*

(Received 6 December 2016; revised manuscript received 18 January 2017; published 10 March 2017)

We combine optical and magneto-optical spectroscopies with complementary vibrational and magnetic property measurements to reveal finite length scale effects in nanoscale α-Fe_2O_3. Analysis of the d-to-d on-site excitations uncovers enhanced color contrast at particle sizes below approximately 75 nm due to size-induced changes in spin-charge coupling that are suppressed again below the superparamagnetic limit. These findings provide a general strategy for amplifying magnetochromism in α-Fe_2O_3 and other iron-containing nanomaterials that may be useful for advanced sensing applications. We also unravel the size dependence of collective excitations in this iconic antiferromagnet.

DOI: 10.1103/PhysRevB.95.125416

I. INTRODUCTION

The interplay between charge, structure, and magnetism is the origin of rich functionality in complex materials. Competing interactions are particularly strong in oxides, giving rise to elaborate T-H-P-$h\nu$ phase diagrams, often with exotic states that derive from delicately balanced coupling [1,2]. Small external perturbations, for instance, magnetic field, pressure, or light, can change important energy and length scales, driving these flexible materials into new areas of phase space with very different properties [3–9]. These competing states are interesting and useful because of their different functionalities. Finite length scale effects also influence the interaction between charge, structure, and magnetism [10–12]. Nanoscale oxides like MnO and $CoFe_2O_4$, for instance, sport modified chemical bonding, displacive transitions, and spin-lattice couplings compared to their bulk analogs [13–15]. Less is known, however, about how size can be used to control spin-charge interactions.

We identified α-Fe_2O_3, commonly known as hematite, as a model antiferromagnet with which to test these ideas. This system displays a spin-flop transition that is driven by both temperature ($T_M = 263$ K) and magnetic field ($H_{SF} = 6$ and 16 T for the easy and hard axis, respectively) [16–18]. Applied field creates color contrast (red $\rightarrow$ red′) via a spin-charge coupling mechanism by amplifying changes in the ${}^6A_{1g} \rightarrow {}^4T_{1g}$ on-site excitation across the spin-flop transition [19,20]. Analysis of the collective excitations on the leading edge of the d-to-d transition also reveals magnetic symmetry [20]. Confinement reduces the overall energy scales—a trend that is easily recognized by the decreased ordering temperatures and critical fields at small sizes [21–23]. It also modifies magnetization [24–28], optical properties [29,30], phonon frequencies [31,32], and vibronic coupling [10]. Complex experimental probes of the fundamental electronic excitations in nanoscale α-Fe_2O_3 and an understanding of how the energy transfer processes involving the charge channel change with size [33,34] are, however, still missing. At the same time, materials that possess a large generalized susceptibility (i.e., a strong response to a small stimulus) are promising candidates for novel device applications. The magnetochromic sensing capabilities explored here thus complement well-known medical and environmental uses of iron oxide nanoparticles [35–38].

In this work, we combine magneto-optical spectroscopy with vibrational and magnetic property measurements to more deeply investigate magnetoelectric coupling in nanoscale hematite. We find stronger field-induced color contrast below approximately 75 nm due to enhanced spin-charge coupling that is suppressed below the super-paramagnetic regime [39]. The spin-charge coupling mechanism also accounts for systematic shifts in the magnon sideband frequency, from which we extract precisely how the fundamental exciton softens with decreasing size. These findings are important for generating large field-induced color contrast in iron-containing earth-abundant materials and emerging magnetochromic sensor applications [40–42].

II. METHODS

Several sizes and shapes of α-Fe_2O_3 nanoparticles were prepared by hydrothermal methods [43–45]. Details on the synthesis, size and distribution analysis, and structural characterization are presented in Ref. [46]. A bulk powder with large micrometer-sized grains was purchased from Alfa Aeser (99.999%) for comparison. The dc magnetization of the α-Fe_2O_3 nanoparticles sealed inside gelatin capsules with paraffin wax was measured after both zero-field cooling and field cooling in a Quantum Design Magnetic Properties Measurement System from 1.8 to 300 K under an applied field of 500 Oe. These results are also shown in the Supplemental

*Corresponding author: musfeldt@utk.edu

Information. For optical transmittance measurements (8700–17 000 cm^{-1}, 2 cm^{-1} resolution), samples were mixed with a matrix and pressed into pellets. Particle concentrations were low, such that interparticle interactions can be neglected. Absorption was calculated as $\alpha(\omega) = \frac{-1}{hd} \ln[T(\omega)]$, where $T(\omega)$ is the measured transmittance, h is the sample loading, and d is thickness. Oscillator strength was calculated as $f = \frac{2c}{N_e \pi \omega_\rho^2} \int_{\omega 1}^{\omega 2} n\alpha(\omega) d\omega$, where $N_e = 5$ is the number of electrons per Fe site, $n \simeq 2.23$ is the refractive index, ω_ρ is the plasma frequency $\omega_\rho \equiv \sqrt{\frac{e^2 \rho}{m \epsilon_0}}$, e and m are the charge and mass of an electron, ϵ_0 is the vacuum dielectric constant, ρ is the density of Fe sites, c is the speed of light, and ω_1 and ω_2 are the frequency limits of integration [47]. The integration range is 10 000–11,000 cm^{-1} for the magnon sideband, and 11 000–14 000 cm^{-1} for the d-to-d excitation. High-field optical (9000–20 800 cm^{-1}, 5 cm^{-1} resolution) and infrared measurements (20–650 cm^{-1}, 2 cm^{-1} resolution) were performed at 4.2 K using a resistive magnet (0–35 T) at the National High Magnetic Field Laboratory in Tallahassee, FL. Raman measurements were taken with a 473-nm laser at 50 mW power and 1800 g/mm grating, integrated between 30 and 60 seconds and averaged three times.

III. RESULTS AND DISCUSSION

A. Magneto-optical properties of hematite nanoparticles

Figures 1(a)–1(c) displays the absorption of polycrystalline α-Fe_2O_3 as well as the response of two different sizes of α-Fe_2O_3 nanoparticles. We assign the broad absorption band centered at 11 600 cm^{-1} as the ${}^6A_{1g} \rightarrow {}^4T_{1g}$ Fe^{3+} on-site excitation [19] and the smaller feature on the leading edge of this structure (at 10 470 cm^{-1}) as a magnon sideband [48]. The former is activated by vibronic coupling and interaction with odd parity phonons whereas the latter is a characteristic dipole-allowed transition that appears in a number of antiferromagnets [19,49–51]. The collective nature of the magnon sideband makes it a superb probe of spin-charge coupling and magnetic quantum phase transitions [20,42]. The magneto-optical response of these materials [also in Figs. 1(a)–1(c)] is shown as a full field absorption difference: $\Delta\alpha = \alpha(35\,T) - \alpha(0\,T)$. This rendering highlights field-induced spectral changes by eliminating commonalities.

Inspection reveals that the absorption difference spectra have the same general shape regardless of particle size, with field-induced changes to both the d-to-d excitation and the magnon side band. A partial sum rule analysis [47] over the appropriate energy windows quantifies these trends [Figs. 1(d)–1(f)]. Prior magneto-optical work on single crystals reveals clear optical contrast through the spin-flop transition with enhancement (and softening) of the magnon sideband and diminution of the on-site excitation due to spin-charge interactions [20]. A remnant of these effects appears in polycrystalline α-Fe_2O_3 and the various nanoparticles of interest here [52]. For example, the oscillator strength of the d-to-d excitation in the bulk powder begins to decrease around 6 T and reaches its steepest slope near 16 T, consistent with the easy and hard axis critical fields of the single crystal [18]. The nanorhombohedra display similar effects although here, the oscillator strength of the color band begins to decrease

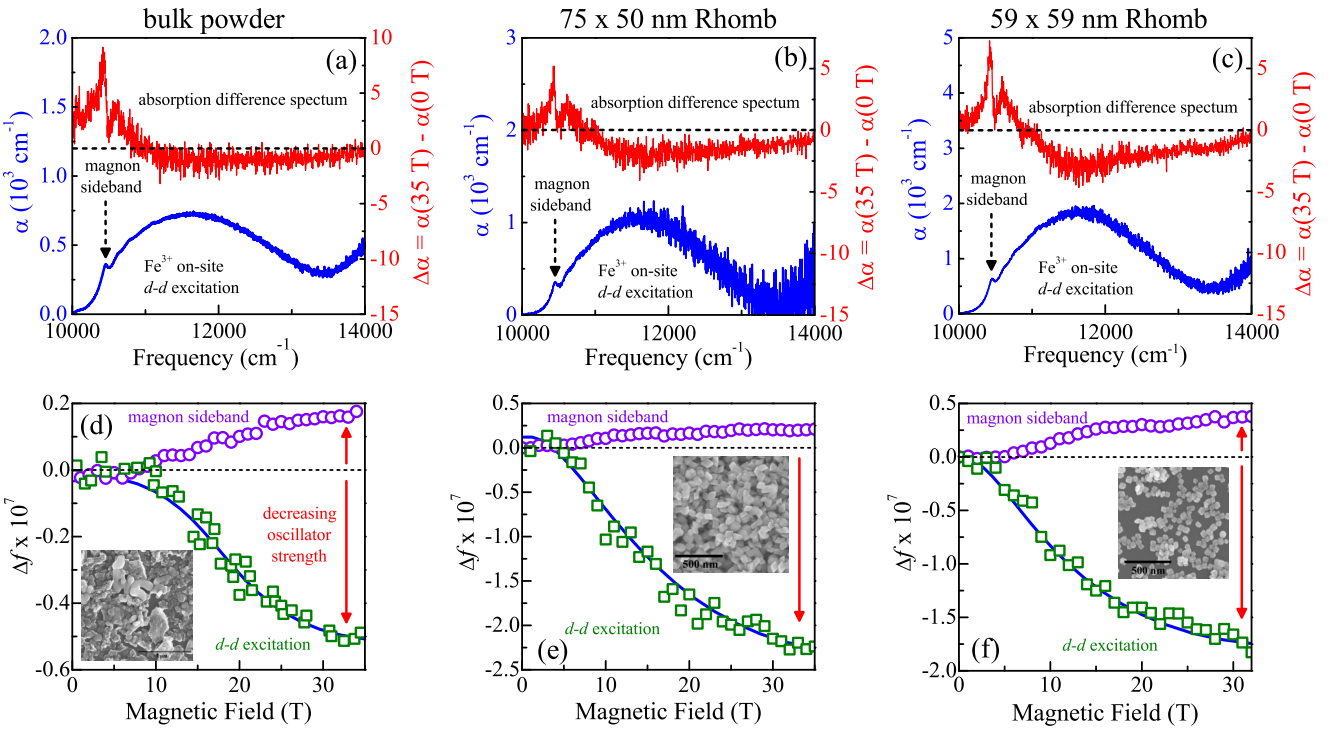

FIG. 1. (a)–(c) 4.2-K absorption spectrum of polycrystalline hematite and selected nanorhombohedra beneath the full field absorption difference spectrum, $\Delta\alpha = \alpha(35\,T) - \alpha(0\,T)$, for comparison. The full data set is available in Ref. [46]. (d)–(f) Change in oscillator strength (Δf) of the d-to-d on-site excitation (green squares) and magnon sideband (violet circles) vs magnetic field for these materials. Blue lines guide the eye.

TABLE I. Summary of the shape, size, and full field absorption difference $\Delta\alpha_{max} = [\frac{\alpha(35\,T)-\alpha(0\,T)}{\alpha(0\,T)}] \times 100$ calculated at the position of the highest absorption, ($\approx$11 600 cm^{-1}) of the hematite nanomaterials used in this work.

material	particle length (nm)	particle width (nm)	$\Delta\alpha_{max}$(%)
bulk powder	$\approx$1000	$\approx$1000	− 1.2
cubes	450 ± 60	450 ± 60	− 1.6
polyhedra	320 ± 90	320 ± 90	− 1.2
rice	148 ± 32	67 ± 10	0
rhombohedra (2x)	105 ± 16	84 ± 12	− 1.5
rhombohedra (L)	75 ± 8	50 ± 7	− 2.1
rhombohedra (M)	59 ± 9	59 ± 8	− 3.1
rhombohedra (S)	50 ± 8	35 ± 7	− 1.9

at lower fields, indicating that smaller fields drive the color change. This is because the critical fields are smaller, in line with direct measurements of H_c [22]. At the same time, a portion of this oscillator strength is transferred to the magnon sideband, which grows with increasing field [Figs. 1(d)–1(f)].

Table I summarizes the magnetochromic response of the full suite of α-Fe_2O_3 nanomaterials of interest (see Fig. S4 in Ref. [46] for data on all samples) [10]. Here, we use the field-induced change in the absorption spectrum ($\Delta\alpha_{max}$) at the center position of the on-site excitation (11 600 cm^{-1}) and highest available field (35 T) to quantitatively compare how the color band changes with size. Inspection of the last column in Table I reveals that, in general, spectral contrast (understood as $|\Delta\alpha_{max}|$) increases with decreasing size—independent of shape.

Figure 2 displays the same data in graphical form. It is easy to identify three distinct regimes: a bulklike regime, a small size range, and an area below the superparamagnetic limit. At large sizes, the field-induced color change is nearly constant and on the order of 1.3% [53]. This is true for the single- and polycrystal as well as for several of the larger nanoparticles including cubes and polyhedra, suggesting that spin-charge coupling (which activates the field-induced color change) is of similar order of magnitude. Things are different when the characteristic particle size drops below about 75 nm ($\approx$60 unit cells). Here, the spectral contrast increases to nearly 3% before dropping back down as the system approaches the super-paramagnetic region [39]. A similar trend emerges for the contrast of the magnon sideband. The enhanced contrast at small size suggests that spin-charge coupling is changing in critical ways - either by systematic enhancement (and subsequent diminishment at the smallest size) or by involving additional degrees of freedom (besides the spin and charge channels). We test these mechanistic scenarios below and find, to our surprise, that spin-charge coupling not only describes the overall trend but provides a plausible explanation for (i) the curious behavior of the smallest nanorhombohedra in this study and (ii) the rigidity of the d-to-d excitation in the nanorice.

B. Mechanism of the field-induced color contrast in α-Fe_2O_3 nanoparticles

It is well established that magnetic field-induced color contrast in hematite single crystals derives from spin-charge coupling that is strongly amplified across the spin-flop transition [20]. It is therefore reasonable to anticipate that a similar mechanism will be relevant to the α-Fe_2O_3 nanoparticles. Our work provides three independent checks of this scenario. The first test involves the behavior of the smallest nanorhombohedra and evaluates the role of the collective transition. Below about 40 nm (close to the size of the smallest rhombohedra), the spin-flop transition does not force spins to lie perfectly along the c axis (as in larger particles) but instead allows a 28° off-axis orientation [54]. This scenario is consistent with the significant moment below the spin-flop transition observed in magnetization measurements of our 35 × 50 nm^2 particles (see Fig. S6 in Ref. [46]), and it suggests that a degraded spin-flop transition might impact magnetochromism. The second check concerns the nanorice sample and even more firmly establishes the importance of the collective transition. Magnetic property measurements of the nanorice reveal no spin-flop transition (see Fig. S7 in Ref. [46]), and correspondingly, magneto-optical experiments up to 35 T (and even test runs to 45 T) show no field-induced absorption difference. In other words, the absence of a spin-flop transition quenches the color contrast. Together, these two results demonstrate that a robust collective transition—in which the spins fully reorient—is required to modify the d-to-d excitation. The final check of the spin-charge coupling mechanism in hematite nanoparticles involves ruling out a lattice contribution. Since the d-to-d excitation is activated by coupling with an odd parity phonon [10], any spin-lattice coupling is expected to involve an infrared-active mode. Direct magneto-infrared measurements

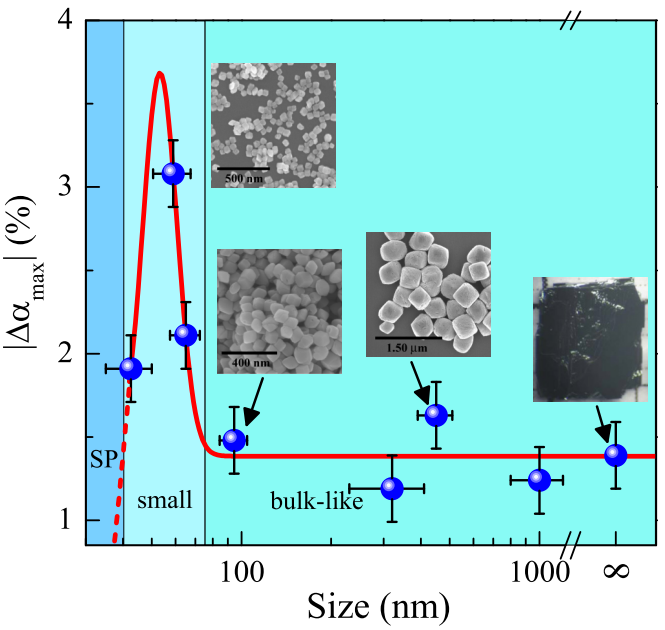

FIG. 2. Full field color contrast, $|\Delta\alpha_{max}| = |\frac{\alpha(35\,T)-\alpha(0\,T)}{\alpha(0\,T)}| \times 100\%$, evaluated at 11 600 cm^{-1} (which corresponds to the maximum of the d-to-d absorption) at 4.2 K. A photo of the single crystal and scanning electron microscope images of select nanoparticles are included. The three different size regimes [bulklike, small size, and superparamagnetic (SP)] are indicated. The red line guides the eye, with the dashed region approximating what may happen at smaller sizes.

of the smallest rhombohedra up to 35 T, however, reveal no local lattice distortions (see Fig. S8 in Ref. [46]), implying that the spin-flop transition occurs without any commensurate changes to the lattice. Taken together, these results show that spin and charge are intimately coupled in α-Fe_2O_3 and can interact directly—without involving the lattice.

C. Magnetochromic sensing applications

In the discussion above, we describe a general strategy for creating enhanced magnetochromic contrast in magnetic nanoparticles like α-Fe_2O_3. It is important to point out that there are a number of applications that can make use of this technology—especially when the color contrast is visible to the human eye. Earth-abundant materials like hematite are inexpensive, safe, and stable. Moreover, small nanoparticles can be mixed into inks and embedded into fibers to provide very subtle and hard-to-duplicate forms of identification of the type that may be useful for anti-counterfeiting purposes. In α-Fe_2O_3, our measurements suggest that particle sizes near 75 nm are likely to produce maximum red $\rightarrow$ red′ magnetochromic color contrast. The magnetic energy scales (as measured by the Morin temperature, for instance) are also relatively high and may be able to support room temperature operation. The latter assumes that the residual spin-spin correlations at room temperature are sufficient to provide a remnant of the collective transition—a supposition that has yet to be tested. Other iron oxides like Fe_3O_4 or $CoFe_2O_4$ will have somewhat different sweet spots, but our research suggests that the size regime just above the transition to the super-paramagnetic state is the place to search for enhanced color contrast that can be observed with a hand-held spectrometer or (even better) by the naked eye. This discovery clearly opens the door to completely new types of sensing from magnetic nanoparticles.

D. Collective excitations and fine structure in α-Fe_2O_3 nanoparticles

Antiferromagnets traditionally offer foundational opportunities for investigating collective excitations like excitons and magnons as well as features like magnon sidebands that arise from charge-spin coupling [50,51,55]. The latter arises from the dipole-allowed combination of an exciton and a magnon ($\omega_{MS} = \omega_E + \omega_M$) and is commonly observed on the leading edge of a d-to-d band [20,48,50,55,56]. Exciton

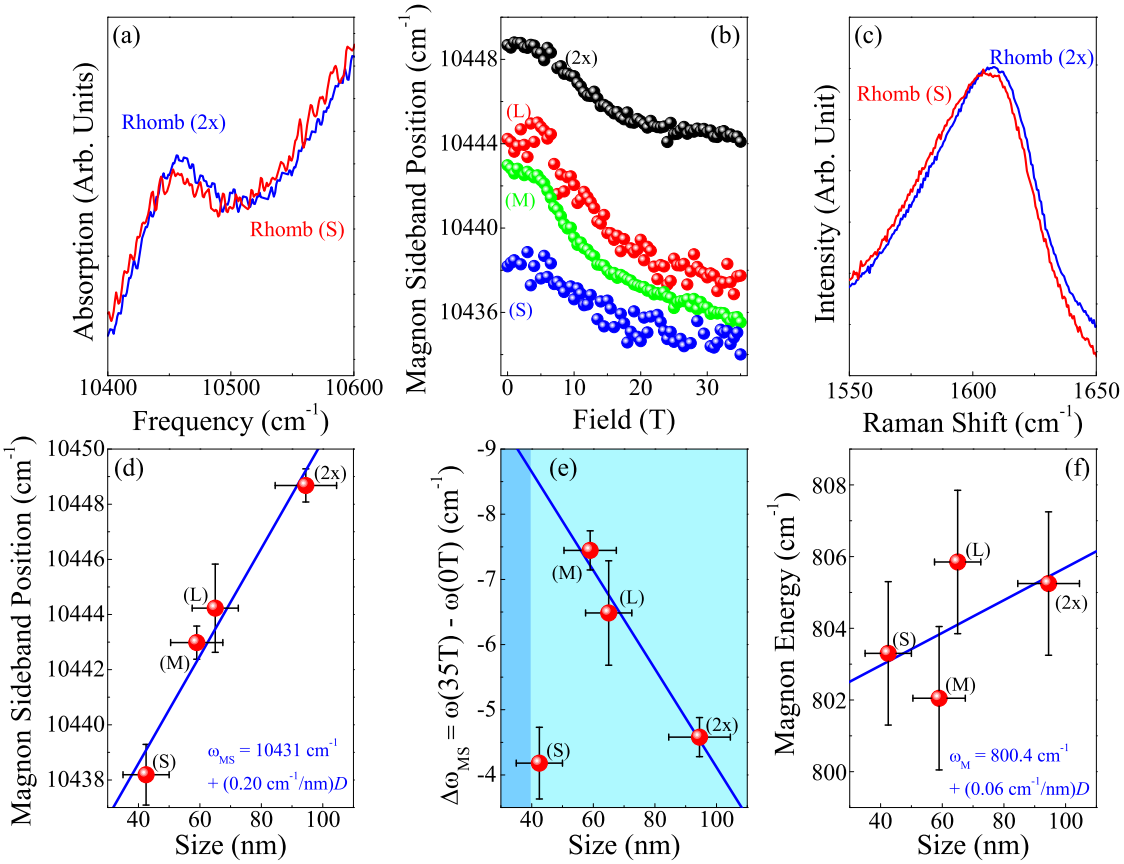

FIG. 3. (a) Magnon sideband for the (blue) largest and (red) smallest rhombohedra. (b) Magnon sideband position vs field for the rhombohedral samples at 4.2 K. (c) Raman-active two magnon mode for the (blue) largest and (red) smallest rhombohedra at 300 K from which the magnon energy was determined. (d) Magnon sideband position vs particle size at 4.2 K and zero field. The equation reveals the limiting "zero size" value of the magnon sideband position and its systematic shift with particle size D in nanometers. (e) Change in magnon sideband position at 35 T vs size. Note that the smallest size particles are close to the super-paramagnetic region. (f) Magnon energy vs size. The limiting "zero size" position of the magnon and estimated linear size-dependent shift are extracted from the indicated fit. The sample specifications are given in Table I.

splitting and magnon sideband trends are incisive probes of symmetry, and their behavior can even be used to develop temperature-magnetic field phase diagrams [20,56,57]. While much is known about excitons, magnons, and magnon sidebands in antiferromagnets under external stimuli, there have been few opportunities to reveal finite length scale effects on the behavior of collective excitations. Our suite of hematite nanoparticles provides a superb platform for such tests [20,48,58].

Figure 3 summarizes how the collective excitations in nanohematite change with size. An obvious linear correlation exists between particle size and magnon sideband position in the absence of magnetic field [Figs. 3(a) and 3(d)]. As particle size decreases, the frequency of the magnon sideband is reduced. This trend is due to the combined size dependence of the exciton and magnon that compose it and, in the discussion below, we separate the two effects. The magnon sideband position also softens through the field-driven spin-flop transition [Fig. 3(b)]. The degree to which the field-induced softening of the magnon sideband $\Delta\omega_{MS}$ depends upon size is interesting [Fig. 3(e)]. $\Delta\omega_{MS}$ increases linearly in the small size regime but weakens again as the superparamagnetic regime is approached. This is because only a remnant of the spin-flop transition survives below the superparamagnetic limit, a situation that we already established as inconsistent with maximum spin-charge coupling [54,59].

Magnons are a type of spin wave commonly found in magnetic materials [60,61] and are typically explored with neutron and Raman scattering techniques. The two-magnon mode, in particular, is Raman-active [62,63]. It is straightforward to estimate the magnon frequency ω_M from measurements of the two magnon mode as $\omega_{2M} = 2\omega_M$. In α-Fe_2O_3 single crystals, this yields $\omega_M = 782\ \mathrm{cm}^{-1}$ [20,64,65]. Figures 3(c) and 3(f) displays the Raman-active two-magnon peak and the size dependence of ω_M (see Fig. S5 in Ref. [46] for all spectra). At least within the rhombohedral sub-class, ω_M is nearly rigid [66]. Since $\omega_{MS} = \omega_E + \omega_M$, simple subtraction reveals that the exciton frequency must also decrease as particle size is reduced. We find $\omega_E = 9631 + (0.14\ \mathrm{cm}^{-1}/\mathrm{nm})D$, where D is particle size in nanometers. Comparison of the relative slopes reveals that the exciton is much more sensitive to size than the magnon [67].

IV. CONCLUSION

We measured the magneto-optical properties of a series of α-Fe_2O_3 nanoparticles in order to reveal finite length scale effects on the fundamental electronic excitations. Decreasing the particle size below 75 nm amplifies the field-induced color contrast due to enhanced spin-charge coupling—until the onset of superparamagnetism quenches the effect. Various mechanistic tests, including the analysis of similar trends in nanorice samples and direct measurement of spin-lattice coupling with magneto-infrared spectroscopy, demonstrate the importance of a robust spin-flop transition; when the spin-flop is incomplete or absent, the color contrast is reduced or suppressed, respectively. We also took the opportunity to explore finite length scale effects on the collective excitations in α-Fe_2O_3 from which we learn that the exciton is much more susceptible to confinement than the magnon. This work advances the understanding of size effects on the color properties of multifunctional materials, motivates the extension to nanoanalogs of materials where different color change mechanisms are at work, and provides a general strategy for creating enhanced magnetochromic responses that are visible to the human eye.

ACKNOWLEDGMENTS

This research is supported by the Materials Science Division, Office of Basic Energy Sciences, U.S. Department of Energy under Awards DE-FG02-01ER45885 (J.L.M., spectroscopy), DE-SC-00112704 (S.S.W., nanoparticle growth and characterization) and DE-SC-00112704 (M.C.A., magnetic properties). Parts of this work were conducted at the National High Magnetic Field Laboratory, which is supported by the National Science Foundation through NSF DMR-1157490 and the State of Florida. J.W.S. was supported by a Provost's Research Fellowship from Farmingdale State College.

[1] N. A. Fortune, S. T. Hannahs, Y. Yoshida, T. E. Sherline, T. Ono, H. Tanaka, and Y. Takano, Phys. Rev. Lett. **102**, 257201 (2009).
[2] S. Haravifard, D. Graf, A. E. Feiguin, C. D. Batista, J. C. Lang, D. M. Silevitch, G. Srajer, B. D. Gaulin, H. A. Dabkowska, and T. F. Rosenbaum, Nat. Commun. **7**, 11956 (2016).
[3] E. Coronado, M. C. Giménez-López, T. Korzeniak, G. Levchenko, F. M. Romero, A. Segura, V. García-Baonza, J. C. Cezar, F. M. F. de Groot, A. Milner, and M. Paz-Pasternak, J. Am. Chem. Soc. **130**, 15519 (2008).
[4] H. Cui, J. S. Brooks, A. Kobayashi, and H. Kobayashi, J. Am. Chem. Soc. **131**, 6358 (2009).
[5] M. K. Liu, B. Pardo, J. Zhang, M. M. Qazilbash, S. J. Yun, Z. Fei, J.-H. Shin, H.-T. Kim, D. N. Basov, and R. D. Averitt, Phys. Rev. Lett. **107**, 066403 (2011).
[6] C. Marini, M. Valentini, A. Perucchi, P. Dore, D. D. Sarma, S. Lupi, and P. Postorino, High Press. Res. **31**, 18 (2011).
[7] T. Aoyama, K. Yamauchi, A. Iyama, S. Picozzi, K. Shimizu, and T. Kimura, Nat. Commun. **5**, 4927 (2014).
[8] K. Lekin, H. Phan, S. M. Winter, J. W. L. Wong, A. A. Leitch, D. Laniel, W. Yong, R. A. Secco, J. S. Tse, S. Desgreniers, P. A. Dube, M. Shatruk, and R. T. Oakley, J. Am. Chem. Soc. **136**, 8050 (2014).
[9] P. Chen, B. S. Holinsworth, K. R. O'Neal, T. V. Brinzari, D. Mazumdar, Y. Q. Wang, S. McGill, R. J. Cava, B. Lorenz, and J. L. Musfeldt, Phys. Rev. B **89**, 165120 (2014).
[10] K. R. O'Neal, J. M. Patete, P. Chen, B. S. Holinsworth, J. M. Smith, N. Lee, S.-W. Cheong, S. S. Wong, C. Marques, M. C. Aronson, and J. L. Musfeldt, J. Chem. Phys. **141**, 044710 (2014).
[11] B. Wei, K. Zheng, Y. Ji, Y. Zhang, Z. Zhang, and X. Han, Nano Lett. **12**, 4595 (2012).
[12] X. Dou, K. Ding, D. Jiang, X. Fan, and B. Sun, ACS Nano **10**, 1619 (2016).

[13] Q. C. Sun, X. Xu, S. N. Baker, A. D. Christianson, and J. L. Musfeldt, Chem. Mater. **23**, 2956 (2011).

[14] Q. C. Sun, S. N. Baker, A. D. Christianson, and J. L. Musfeldt, Phys. Rev. B **84**, 014301 (2011).

[15] Q. C. Sun, C. S. Birkel, J. Cao, W. Tremel, and J. L. Musfeldt, ACS Nano **6**, 4876 (2012).

[16] S. Foner and Y. Shapira, Phys. Lett. A **29**, 276 (1969).

[17] Y. Shapira, Phys. Rev. **184**, 589 (1969).

[18] T. Kaneko and S. Abe, J. Phys. Soc. Japan **20**, 2001 (1965).

[19] L. A. Marusak, R. Messier, and W. B. White, J. Phys. Chem. Solids **41**, 981 (1980).

[20] P. Chen, N. Lee, S. McGill, S.-W. Cheong, and J. L. Musfeldt, Phys. Rev. B **85**, 174413 (2012).

[21] N. Amin and S. Arajs, Phys. Rev. B **35**, 4810 (1987).

[22] R. D. Zysler, D. Fiorani, A. M. Testa, L. Suber, E. Agostinelli, and M. Godinho, Phys. Rev. B **68**, 212408 (2003).

[23] The Morin temperature disappears at sizes below 8 nm in α-Fe_2O_3 [21,22].

[24] R. Kodama and A. Berkowitz, Phys. Rev. B **59**, 6321 (1999).

[25] A.-H. Lu, E. L. Salabas, and F. Schüth, Angew. Chemie Int. Ed. **46**, 1222 (2007).

[26] T.-J. Park, G. C. Papaefthymiou, A. J. Viescas, A. R. Moodenbaugh, and S. S. Wong, Nano Lett. **7**, 766 (2007).

[27] C. de Montferrand, Y. Lalatonne, D. Bonnin, N. Liévre, M. Lecouvey, P. Monod, V. Russier, and L. Motte, Small **8**, 1945 (2012).

[28] K. Woo, J. Hong, S. Choi, H.-W. Lee, J.-P. Ahn, C. S. Kim, and S. W. Lee, Chem. Mater. **16**, 2814 (2004).

[29] R. Koole, G. Allan, C. Delerue, A. Meijerink, D. Vanmaekelbergh, and A. J. Houtepen, Small **4**, 127 (2008).

[30] N. Shirahata, T. Hasegawa, Y. Sakka, and T. Tsuruoka, Small **6**, 915 (2010).

[31] I. V. Chernyshova, M. F. Hochella Jr., and A. S. Madden, Phys. Chem. Chem. Phys. **9**, 1736 (2007).

[32] P. Chen, X. Xu, C. Koenigsmann, A. C. Santulli, S. S. Wong, and J. L. Musfeldt, Nano Lett. **10**, 4526 (2010).

[33] F. J. Owens and J. Orosz, Solid State Commun. **138**, 95 (2006).

[34] A. C. Gandhi, J. Pant, S. D. Pandit, S. K. Dalimbkar, T.-S. Chan, C.-L. Cheng, Y.-R. Ma, and S. Y. Wu, J. Phys. Chem. C **117**, 18666 (2013).

[35] G. Liu, J. Gao, H. Ai, and X. Chen, Small **9**, 1533 (2013).

[36] H. J. Shipley, K. E. Engates, and A. M. Guettner, J. Nanoparticle Res. **13**, 2387 (2011).

[37] S. Laurent, D. Forge, M. Port, A. Roch, C. Robic, L. Vander Elst, and R. N. Muller, Chem. Rev. **108**, 2064 (2008).

[38] A. K. Gupta and M. Gupta, Biomaterials **26**, 3995 (2005).

[39] T. P. Raming, A. J. S. Winnubst, C. M. van Kats, and A. P. Philipse, J. Colloid Interface Sci. **249**, 346 (2002).

[40] X. Chen, L. Li, X. Sun, Y. Liu, B. Luo, C. Wang, Y. Bao, H. Xu, and H. Peng, Angew. Chemie Int. Ed. **50**, 5486 (2011).

[41] J. Ge, H. Lee, L. He, J. Kim, Z. Lu, H. Kim, J. Goebl, S. Kwon, and Y. Yin, J. Am. Chem. Soc. **131**, 15687 (2009).

[42] X. S. Xu, T. V. Brinzari, S. Lee, Y. H. Chu, L. W. Martin, A. Kumar, S. McGill, R. C. Rai, R. Ramesh, V. Gopalan, S. W. Cheong, and J. L. Musfeldt, Phys. Rev. B **79**, 134425 (2009).

[43] Z. Pu, M. Cao, J. Yang, K. Huang, and C. Hu, Nanotechnology **17**, 799 (2006).

[44] C.-J. Jia, L.-D. Sun, Z.-G. Yan, L.-P. You, F. Luo, X.-D. Han, Y.-C. Pang, Z. Zhang, and C.-H. Yan, Angew. Chemie Int. Ed. **44**, 4328 (2005).

[45] T. J. Park and S. S. Wong, Chem. Mater. **18**, 5289 (2006).

[46] See Supplemental Material at http://link.aps.org/supplemental/10.1103/PhysRevB.95.125416 for nanoparticle synthesis and characterization, comparison to single-crystal data, magneto-optical spectra and oscillator strength trends for samples not shown, Raman spectra of the two-magnon mode, magnetization data, and magnetoinfrared spectra of the smallest rhombohedra.

[47] F. Wooten, *Optical Properties of Solids* (Academic Press, New York-London, 1972).

[48] A. I. Galuza, A. B. Beznosov, and V. V. Eremenko, Low Temp. Phys. **24**, 726 (1998).

[49] L. L. Lohr Jr., Coord. Chem. Rev. **8**, 241 (1972).

[50] R. L. Greene, D. D. Sell, W. M. Yen, and A. L. Schawlow, Phys. Rev. Lett. **15**, 656 (1965).

[51] D. D. Sell, R. L. Greene, and R. M. White, Phys. Rev. **158**, 489 (1967).

[52] The field-induced spectral trends in the bulk powder and hematite nanoparticles are similar but smeared out compared to what is observed in single crystals [20]. This is due to the intrinsic random crystallite orientation and the distribution of particle sizes—particularly for the highly directional collective excitations.

[53] The single-crystal data is taken from the average of the three polarizations reported previously in Ref. [20].

[54] S.-H. Gee, Y.-K. Hong, J. C. Sur, D. W. Erickson, M. H. Park, and F. Jeffers, IEEE Trans. Magn. **40**, 2691 (2004).

[55] R. M. White and W. M. Yen, Low Temp. Phys. **31**, 777 (2005).

[56] P. Chen, O. Günaydın-Şen, W. J. Ren, Z. Qin, T. V. Brinzari, S. McGill, S.-W. Cheong, and J. L. Musfeldt, Phys. Rev. B **86**, 014407 (2012).

[57] D. D. Sell, J. Appl. Phys. **39**, 1030 (1968).

[58] Here, we focus our discussion on trends in the rhombohedral nanoparticles in order to rule out shape effects [68,69].

[59] That magnon sideband softening trends mirror the size-dependent trends of the absorption difference is a perfect illustration of the common underlying mechanism.

[60] C. E. Patton, Phys. Rep. **103**, 251 (1984).

[61] V. V. Eremenko, Y. G. Litvinenko, and E. V. Matyushkin, Phys. Rep. **132**, 55 (1986).

[62] J. López-Sánchez, A. Serrano, A. Del Campo, M. Abuín, O. Rodríguez de la Fuente, and N. Carmona, Chem. Mater. **28**, 511 (2016).

[63] P. A. Fleury and R. Loudon, Phys. Rev. **166**, 514 (1968).

[64] M. J. Massey, U. Baier, R. Merlin, and W. H. Weber, Phys. Rev. B **41**, 7822 (1990).

[65] E. J. Samuelsen and G. Shirane, Phys. Status Solidi **42**, 241 (1970).

[66] The shift to higher frequency compared to the bulk value is in agreement with a previous report of magnon hardening in α-Fe_2O_3 nanoparticles [33], although trends in particles of similar shape have not yet been reported.

[67] Unfortunately, the fundamental excitons are not directly observed in the spectra due to their high directionality and the intrinsic random orientation of the nanoparticles, so no internal check of the trend is available at this time.

[68] L. Suber, A. G. Santiago, D. Fiorani, P. Imperatori, A. M. Testa, M. Angiolini, A. Montone, and J. L. Dormann, Appl. Organomet. Chem. **12**, 347 (1998).

[69] S. Mitra, S. Das, S. Basu, P. Sahu, and K. Mandal, J. Magn. Magn. Mater. **321**, 2925 (2009).

Supporting Information for "Magnetochromic Sensing and Size-Dependent Collective Excitations in Iron Oxide Nanoparticles"

Kenneth R. O'Neal,[†] Jonathan M. Patete,[‡] Peng Chen,[†] Ruhani Nanavati,[‡,¶] Brian S. Holinsworth,[†] Jacqueline M. Smith,[‡,¶] Carlos Marques,[§] Jack W. Simonson,[‖] Meigan C. Aronson,[¶,§] Stephen A. McGill,[⊥] Stanislaus S. Wong,[‡,¶] and Janice L. Musfeldt[*,†,#]

†*Department of Chemistry, University of Tennessee, Knoxville, Tennessee 37996, USA*

‡*Department of Chemistry, State University of New York at Stony Brook, Stony Brook, New York 11794-3400, USA*

¶*Condensed Matter Physics and Materials Science Division, Brookhaven National Laboratory, Upton, New York 11973, USA*

§*Department of Physics and Astronomy, Stony Brook University, Stony Brook, New York 11794-3800, USA*

‖*Department of Physics, Farmingdale State College, Farmingdale, NY 11735, USA*

⊥*National High Magnetic Field Laboratory, Tallahassee, Florida 32310, USA*

#*Department of Physics, University of Tennessee, Knoxville, Tennessee 37996, USA*

E-mail: musfeldt@utk.edu

Nanoparticle Synthesis and Characterization

Various hematite nanoparticles were prepared in order to investigate the size- and shape-

dependent optical properties. Table S1 summarizes the size and shape of all the materials used in this work. Anhydrous ferric chloride (EM Science, 98+%) was employed as the Fe^{3+} source for all reactions in this work. Growth directing agents include cetyltrimethylammonium bromide (Acros, 99+%) for nanocubes and nanorhombohedra, ammonium dihydrogen phosphate (Aldrich, 99%) for the nanorice, and nonylphenol ethoxylate for the polyhedra. The water used for synthesizing the particles was distilled and deionized. All chemical materials were utilized as received without further purification.

Table S1: Summary of nanoparticles investigated in this work. Size distributions of particles range from 7 to 90 nm.

Shape	Particle Length	Particle Width	Surfactant
Single crystal	42 μm	-	-
Bulk powder	~1000 nm	-	-
Cube	450 nm	450 nm	CTAB[1]
Polyhedra	320 nm	-	NP-9[2]
Rice	148 nm	67 nm	Phosphate ions
Rhombohedra	106 nm	61 nm	CTAB
Rhombohedra	75 nm	50 nm	CTAB
Rhombohedra	59 nm	59 nm	CTAB
Rhombohedra	50 nm	35 nm	CTAB

We adapted a previously reported hydrothermal method to synthesize nanocubes and nanorhombohedra of various sizes.[S1] For the production of our smallest nanorhombohedra (35 x 50 nm), a 0.02 M aqueous solution of cetyltrimethylammonium bromide (CTAB) was stirred until the solution turned clear. The anhydrous $FeCl_3$ precursor was then added to the solution so that the concentration ratio of Fe^{3+} to surfactant was 1:4. The solution was stirred until all precursors were fully dissolved, and then delivered to a Teflon-lined stainless steel autoclave. The autoclave was filled to 80% of the volume capacity with the precursor solution and then maintained at 120 °C for 12 hours. The size of the nanorhombohedra was suitably increased (to 50 x 75 nm) by doubling the concentration of both CTAB and $FeCl_3$, while maintaining the same concentration ratio. An intermediate size of rhombohedra (59 x 59 nm) was synthesized by reacting the latter precursor solution at an adjusted temperature of 100 °C. Meanwhile, our largest rhombohedra sample (61 x 106 nm) was obtained by

increasing the concentration of $FeCl_3$ to 0.02 M with an $FeCl_3$:CTAB precursor ratio of 1:2. Similarly, nanocubes were generated by further increasing the concentration of $FeCl_3$ to 0.05 M so that the concentration ratio of Fe^{3+} to surfactant was 5:4. The product was collected after the autoclaves were cooled to room temperature naturally and subsequently washed with distilled water and ethanol (Acros, 99.5%) by centrifugation.

Truncated one-dimensional nanostructures, which we call "nanorice," were generated by the hydrothermal reaction of ferric chloride and ammonium dihydrogen phosphate.[S2] Specifically, 4.0 mL of a 0.5 M aqueous solution of ferric chloride was mixed with 3.6 mL of a 0.02 M aqueous solution of ammonium dihydrogen phosphate and subsequently diluted to 100 mL. The solution was added to a Teflon-lined stainless steel autoclave at 80% volume capacity. The autoclave was maintained at 220 °C for 2 hours and then cooled to room temperature naturally. The precipitate was collected and washed with distilled water and ethanol by centrifugation.

The polyhedra evaluated in this work were prepared by a molten salt synthesis.[S3] Specifically, commercial iron oxide nanoparticles (Aldrich) were mixed with NaCl (Mallinckrodt) and nonylphenol ethoxylate (NP-9) (Aldrich), in a 1:40:6 molar ratio. The precursor materials were ground together in an agate mortar for 30 minutes and subsequently sonicated before being placed into a porcelain coated ceramic crucible. The sample was then annealed in a tube furnace at 820 °C for 3.5 hours and allowed to cool down to room temperature at a natural rate. The ramp rate of the tube furnace was set to 5 °C/min. The as-prepared particles were isolated from the salt matrix by washing the product with distilled water, and ultimately collected with centrifugation.

The composition and crystallinity of our as-prepared products were investigated by x-ray powder diffraction. Diffraction patterns were obtained on a Scintag diffractometer operating in the Bragg-Bretano configuration using Cu Kα radiation ($\lambda = 1.54$ Å) from 20 to 70 ° at a scanning rate of 0.50 ° per minute (Fig. S1). To investigate the size and morphology of our as-prepared nanoparticles, the product was dispersed in ethanol by sonication and drop cast

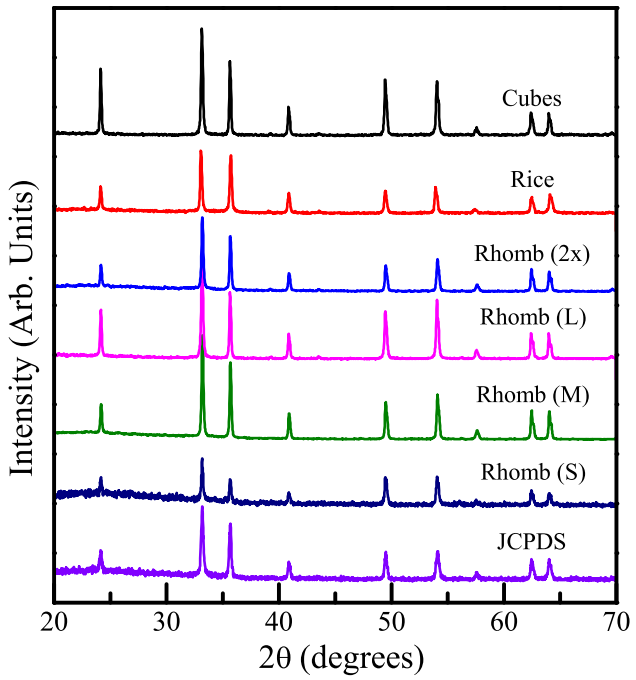

Figure S1: X-ray diffraction patterns for each nanoparticle sample, compared with the JCPDS standard pattern for α-Fe_2O_3 demonstrating the crystallinity and purity of the produced nanoparticles.

onto a clean silicon wafer. The substrates were imaged with a Hitachi S-4800 field-emission scanning electron microscope operating at an accelerating voltage of 5 kV (Fig. S2).

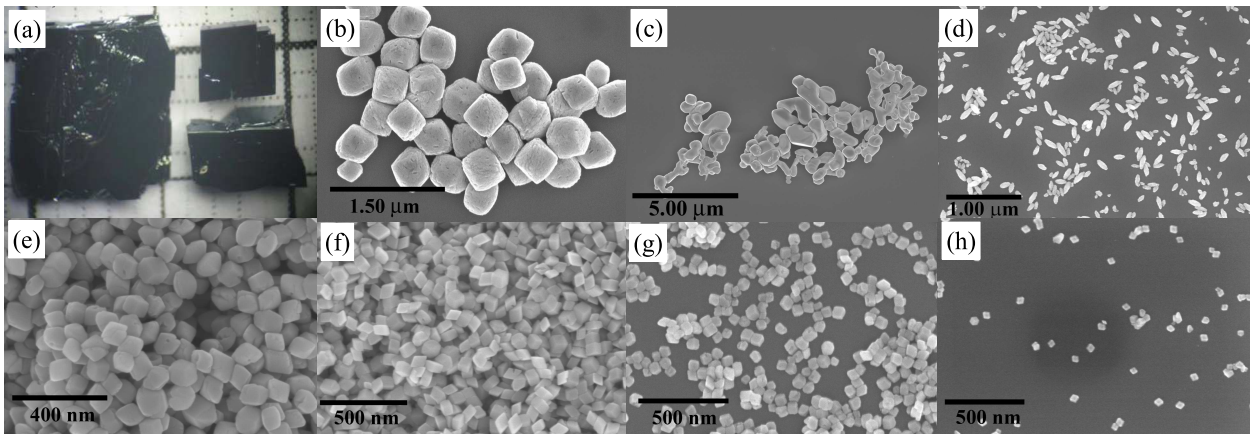

Figure S2: (a) Photographs of the single crystals. The grid lines represent 1 mm each. Scanning electron microscope images of the (b) nanocubes, (c) polyhedra, (d) nanorice, and (e-h) nanorhombohedra from largest to smallest.

Comparing the single crystal and isotropic bulk powder data

In order to compare our randomly oriented α-Fe_2O_3 nanoparticle samples to the polarized

single crystal measurements [Fig. S3 (a)], a bulk powder was measured where all polarizations are observed simultaneously. Averaging the three polarizations of the single crystal[S4] [Fig. S3 (b)] yields an absorption and a 35 T field-induced absorption difference with the same general lineshape as the bulk powder [Fig. S3 (c)]. Tracking the oscillator strength changes versus magnetic field for the polarized single crystal reveals sharp changes around the critical fields of 6 and 16 T for the easy and hard axes, respectively [Fig. S3 (d)]. When a simple average is taken [Fig. S3 (e)], these discontinuities smear out as observed in the bulk powder [Fig. S3 (f)].

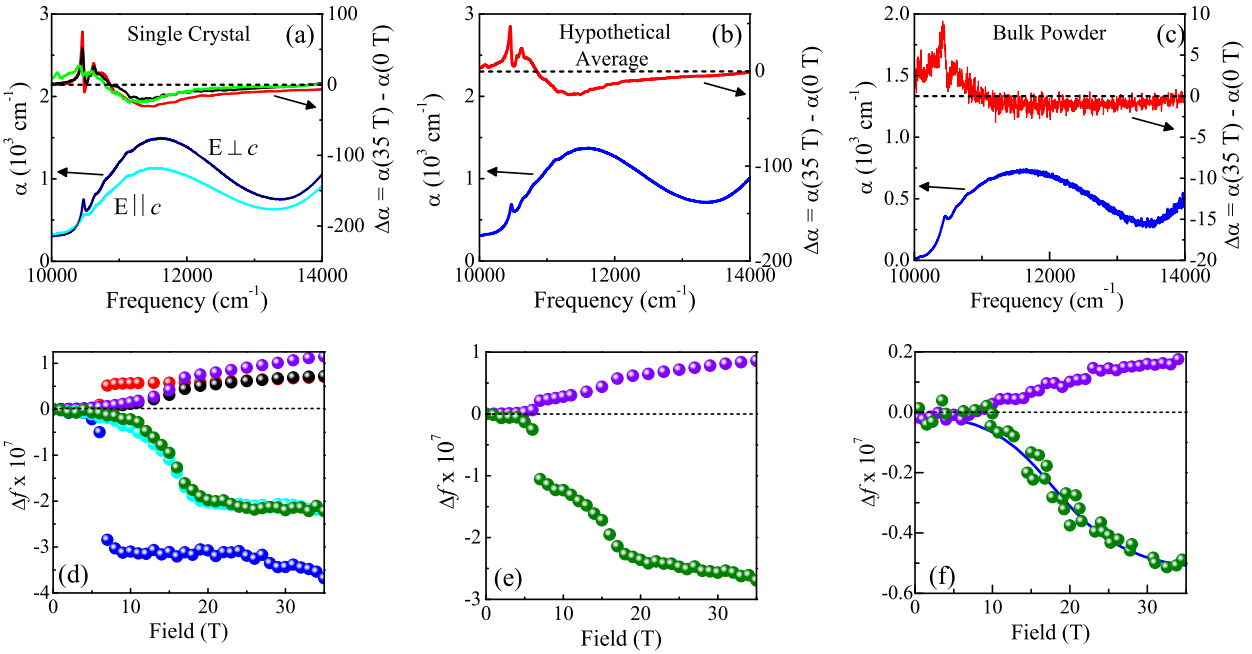

Figure S3: Absorption for the (a) single crystal at 4.2 K and difference polarizations, where red is the absorption difference within the *ab* plane, and black and green are within the *ac* plane with magnetic field along *a* and *c*, respectively. (b) average of the three polarizations of the single crystal, and (c) isotropic bulk powder. Oscillator strength for (d) polarized single crystal where the colors correspond to the polarizations in (a), (e) averaged single crystal, and (f) bulk powder. Curves with positive values are related to the magnon sideband, while the *d*-to-*d* excitation oscillator strength decreases. The absorption difference shape and field dependence are in reasonable agreement with the average of the polarized single crystal data. Single crystal data is reproduced from Ref. S4.

Magnetic field-induced optical absorption differences of α-Fe_2O_3 nanoparticles

The main text highlighted optical spectra and field-induced trends for select samples as examples. Figure S4 displays the spectra, field-induced absorption differences, and oscillator

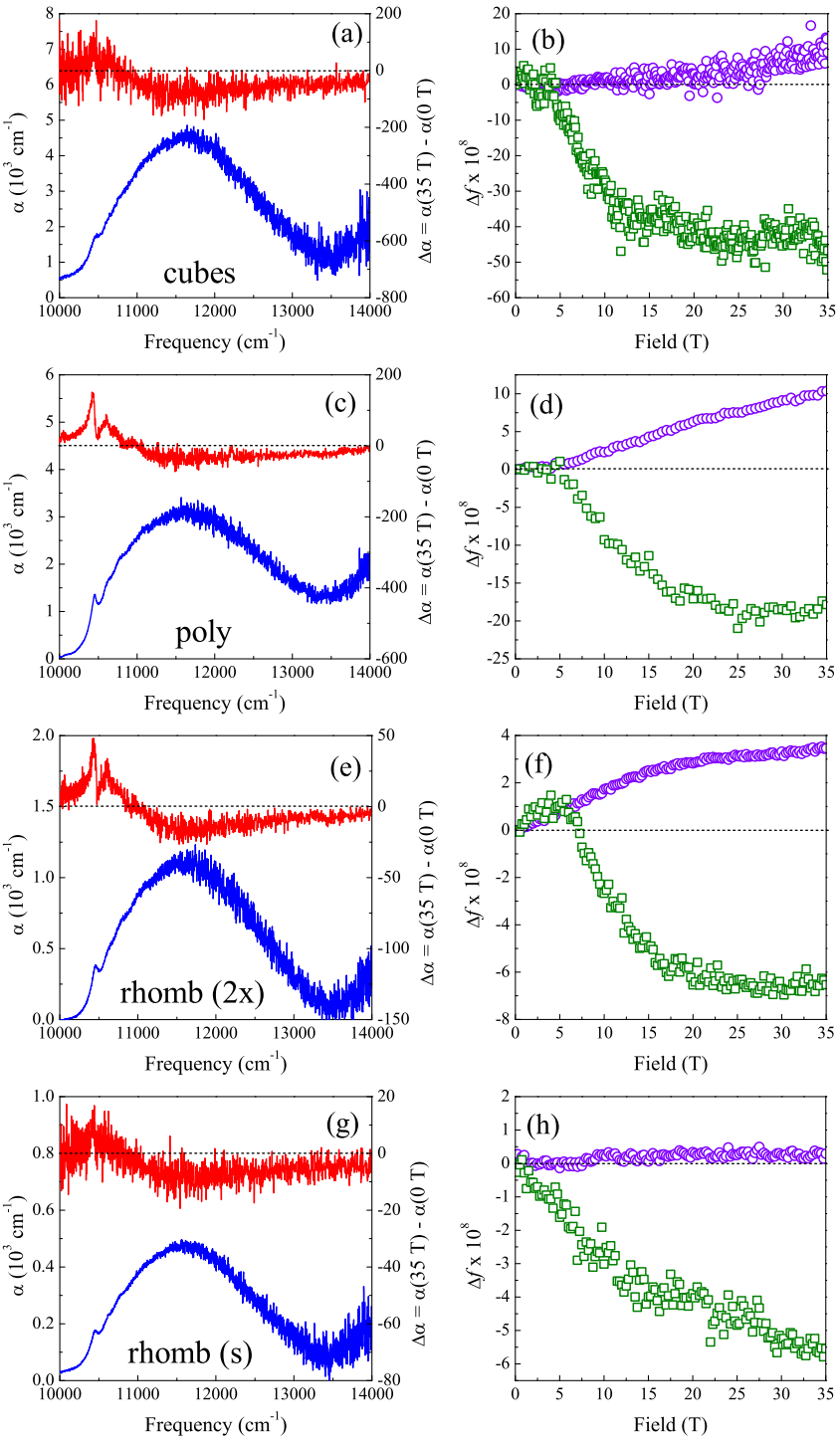

Figure S4: (left) 4.2 K absorption and 35 T magnetic field-induced absorption difference for various α-Fe_2O_3 nanoparticles. (right) Oscillator strength trends for the $d-d$ excitation and magnon sideband for the corresponding samples.

strength trends for the remaining samples. It is again apparent that all samples display the same general trends: decreased absorption of the $d-d$ excitation and increased oscillator strength of the magnon sideband through the spin-flop transition.

Probing the magnon energy via Raman spectroscopy

The Raman spectrum of α-Fe_2O_3 contains a two magnon mode, from which the magnon energy can be extracted. Figure S5 displays a portion the Raman spectra of the rhombohedral nanoparticles. Each sample display a peak near 1600 cm^{-1} which we assign as the two magnon mode. Fitting this peak to extract the frequency allows the back-calculation of the magnon energy, as discussed in the main text.

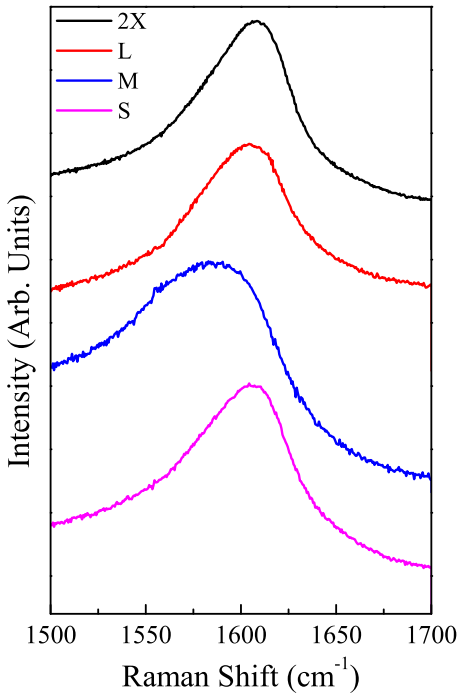

Figure S5: Raman spectra of the rhombohedral α-Fe_2O_3 nanoparticles focusing on the region of the two magnon mode.

Testing the spin-charge coupling mechanism

In an effort to understand the mechanism of the field-induced changes in our α-Fe_2O_3 nanoparticles, we measured the magnetization from 1.8 to 300 K focusing on the rhombohedral samples to eliminate shape effects (Fig. S6). In both the field-cooled and zero

field-cooled cases the magnetization shows a drop below the Morin transition ($T_M \approx 250\ K$) indicating the spin-flop. The magnitude of this drop becomes smaller with decreasing size as both the magnetization above T_M is reduced and the magnetization below this temperature is enhanced. The smallest rhombohedral sample displays a significant magnetization below T_M, in line with spins lying off-axis in nanoparticles smaller than 40 nm.[S5]

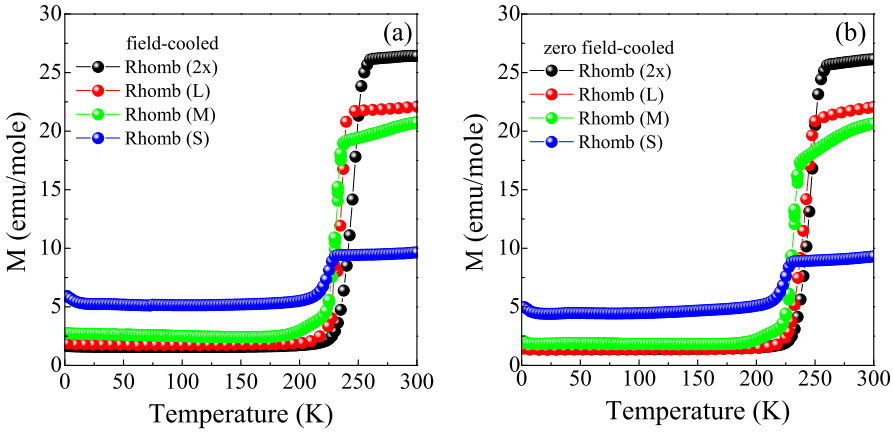

Figure S6: (a) Field-cooled and (b) zero field-cooled magnetization of the rhombohedral α-Fe_2O_3 nanoparticles. Here, we employ the sample designations as given in Table 1 of the main text.

While the rhombohedral samples all display a field-induced color change, the nanorice exhibits no such effect up to 45 T [Fig. S7 (a)]. Again, the magnetic properties explain this behavior. Magnetization measurements [Fig. S7 (b)] show the absence of the spin-flop transition in both the field-cooled and zero field-cooled cases, in agreement with acicular nanoparticles before sintering.[S6] This indicates that the field-driven spin-flop transition, where the spins fully reorient, is necessary for the absorption difference to occur.

Although the nanorice data indicate that the collective magnetic transition plays a main role in the field-induced absorption difference, we wanted to understand the role of the lattice since field-driven spin-flops can drive lattice distortions in oxides.[S7] We measured the infrared response (Fig. S8) of the smallest nanoparticles to search for signs of magnetoelastic coupling. Even up to 35 T there are no features in the infrared absorption difference (Fig. S8), indicating that the lattice is not affected by the spin-flop. Spin-lattice coupling can

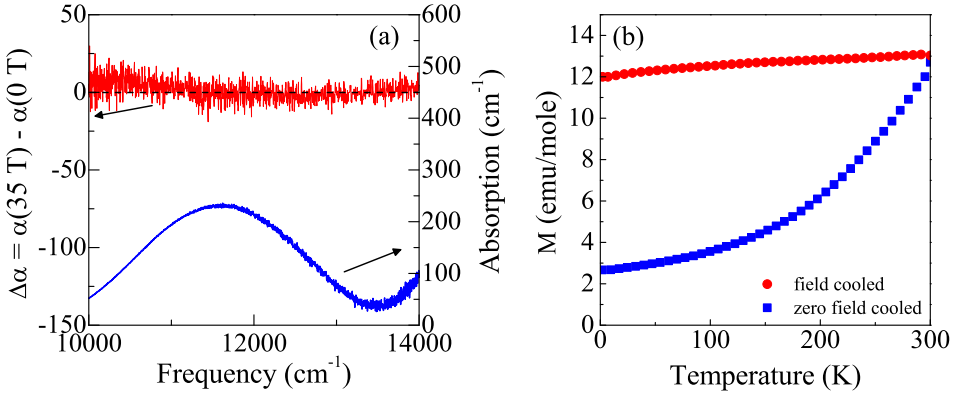

Figure S7: (a) 4.2 K absorption (blue) and 45 T absorption difference (red) for the nanorice displaying no features. (b) Magnetization versus temperature showing the lack of the spin-flop transition.

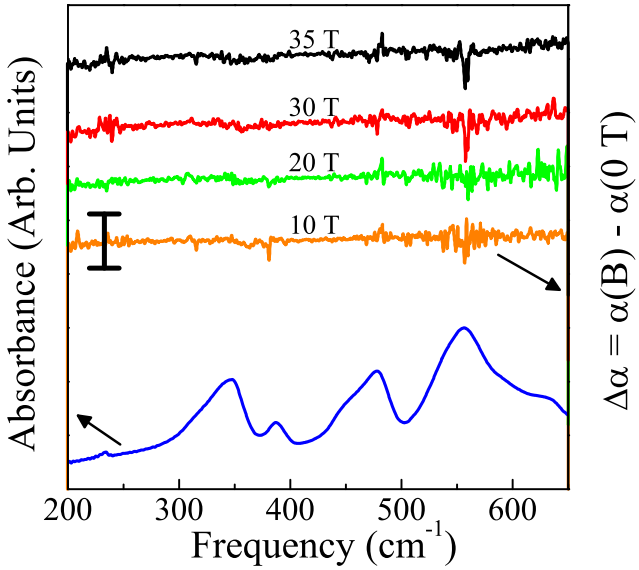

Figure S8: 4.2 K far infrared spectrum of the smallest rhombohedral sample (blue) and absorption differences at the indicated fields. Absorption difference spectra are offset for clarity, and the scale bar represents 50 cm^{-1}.

then be ruled out as a contributing factor of the color contrast.

Combined, the lack of absorption difference in the nanorice and the rigidity of the lattice in the nanorhombohedra demonstrate that the mechanism of the field-induced color change is simply spin-charge coupling. The spin-flop transition is required to observe the high field absorption difference, and the spin-flop does not affect the lattice. This leaves only spin-charge coupling as the underlying mechanism.

References

[S1] Pu, Z.; Cao, M.; Yang, J.; Huang, K.; Hu, C. Controlled synthesis and growth mechanism of hematite nanorhombohedra, nanorods and nanocubes. *Nanotechnology* **2006**, *17*, 799–804.

[S2] Jia, C.-J.; Sun, L.-D.; Yan, Z.-G.; You, L.-P.; Luo, F.; Han, X.-D.; Pang, Y.-C.; Zhang, Z.; Yan, C.-H. Single-crystalline iron oxide nanotubes. *Angew. Chemie - Int. Ed.* **2005**, *44*, 4328–4333.

[S3] Park, T. J.; Wong, S. S. As-prepared single-crystalline hematite rhombohedra and subsequent conversion into monodisperse aggregates of magnetic nanocomposites of iron and magnetite. *Chem. Mater.* **2006**, *18*, 5289–5295.

[S4] Chen, P.; Lee, N.; McGill, S.; Cheong, S.-W.; Musfeldt, J. L. Magnetic-Field-Induced Color Change in α-Fe_2O_3 Single Crystals. *Phys. Rev. B* **2012**, *85*, 174413.

[S5] Gee, S. H.; Hong, Y. K.; Sur, J. C.; Erickson, D. W.; Park, M. H.; Jeffers, F. Spin Orientation of Hematite (α-Fe_2O_3) Nanoparticles During the Morin Transition. *IEEE Trans. Magn.* **2004**, *40*, 2691–2693.

[S6] Suber, L.; Santiago, A. G.; Fiorani, D.; Imperatori, P.; Testa, A. M.; Angiolini, M.; Montone, A.; Dormann, J. L. Structural and Magnetic Properties of α-Fe_2O_3 Nanoparticles. *Appl. Organomet. Chem.* **1998**, *12*, 347–351.

[S7] Yokosuk, M. O.; Artyukhin, S.; al-Wahish, A.; Wang, X.; Yang, J.; Li, Z.; Cheong, S.-W.; Vanderbilt, D.; and Musfeldt, J. L., Tracking the Continuous Spin-Flop Transition in Ni_3TeO_6 by Infrared Spectroscopy. *Phys. Rev. B* **2015**, *92*, 144305.